



Temperature Effects on the Electrodeposition of Zinc

Jingxian Yu,^z Lei Wang, Lei Su, Xinping Ai, and Hanxi Yang

Research Center of Electrochemical Engineering, Department of Chemistry, Wuhan University,
Wuhan 430072, China

The temperature dependence of the cyclic voltammetric profiles for the reduction of zinc into a static mercury drop electrode and the electrocrystallization of zinc onto a glassy carbon (GC) electrode have been examined using cyclic voltammetry and chronoamperometry, respectively. The quasi-two-dimensional growth and the microstructure of the deposited zinc film have also been characterized by video camera and scanning electron microscopy (SEM). The kinetic parameters D , α , and k for the $\text{Zn}^{2+} + 2e^- = \text{Zn(Hg)}$ reaction were calculated at three temperatures. Their values increase with increasing temperature. According to the slope, $d \ln kd(1/T)$, we determined the activation energy of the $\text{Zn}^{2+} + 2e^- = \text{Zn(Hg)}$ reaction to be $-39.662 \text{ kJ mol}^{-1}$. On the other hand, the chronoamperometric results showed that the nucleation density increases when the temperature increases. Moreover, the nucleation rate constant, A , is always very large at different temperatures, about $1.41 \times 10^9 \text{ s}^{-1}$. This indicates that the mechanism of zinc electrocrystallization onto a GC electrode follows a three-dimensional (3-D) instantaneous nucleation and growth model within the controlled temperature range. As for the quasi-2-D growth forms and the microstructure of the zinc deposit, the experimental results showed that the fractal morphology of zinc exhibits isotropic growth with more and thicker branches at 273 K. In contrast, the fractal morphology of zinc exhibits anisotropic growth with fewer and thinner branches at 323 K. Similarly, the results obtained for the microstructure of the zinc deposit showed that plate-like crystals grow unintegrally like irregular hexagonal crystallites at 273 K, but the grains develop integrally and adequately at 323 K.
© 2002 The Electrochemical Society. [DOI: 10.1149/1.1525269] All rights reserved.

Manuscript submitted October 11, 2001; revised manuscript received July 15, 2002. Available electronically November 21, 2002.

The electrodeposition of zinc has gained much attention in the past twenty years, because it is strongly related to the properties of electrodeposited zinc surface and the lifetime of secondary zinc electrodes. Our earlier studies¹⁻³ showed that organic additives can not only change the electrocrystallization mechanism of zinc, but also affect the morphology and texture of the deposited film and give rise to crystalline defects. By the use of selected organic additives, Zhou and his co-workers⁴ prepared zinc deposits with a highly preferred orientation. Hibbert *et al.*⁵ investigated the chemical effects of several polymer supported membranes on morphology of the two-dimensional (2-D) growth. Although the zinc electrodeposition mechanisms are well known, the temperature effects on the electrodeposition are seldom reported.

In this paper, the temperature dependence of the cyclic voltammetric profiles for the reduction of zinc into a static mercury drop electrode was determined at different temperatures. The electrodeposition of zinc onto a glassy carbon (GC) electrode was examined using chronoamperometry. Meanwhile the quasi-2-D growth forms and the microstructure of the deposited zinc film were characterized by a video camera and scanning electron microscopy (SEM).

Experimental

All of the cyclic voltammograms (CVs) were carried out using a static mercury drop working electrode. The electrolyte was an aqueous solution of $0.1 \text{ mol L}^{-1} \text{ Zn(Ac)}_2$ with $0.5 \text{ mol L}^{-1} \text{ NaAc}$ (Ac is acetate). The secondary electrode was a Pt wire with a large surface area. All potentials were reported with respect to the saturated calomel electrode (SCE). All of the chronoamperometric experiments were performed in the solution of $0.1 \text{ mol L}^{-1} \text{ Zn(Ac)}_2$ with $0.5 \text{ mol L}^{-1} \text{ NaAc}$. The working electrode was a Teflon-shrouded GC rod, 2 mm in diam. A 99.9% pure zinc sheet was used as the counter electrode. Prior to each experiment, the working electrode was polished to a mirror finish with successively finer grades of alumina powders, eventually to $0.05 \mu\text{m}$, and then ultrasonically cleaned in acetone, dilute aqueous HCl, and distilled water. The step potentials were provided and corresponding current transients were recorded simultaneously by computer. The initial potential for all chronoamperometric experiments was set to -1.00 V . During the experiments, the electrochemical cells were immersed in a water bath, and the temperature was controlled within $\pm 1.0 \text{ K}$ by means of

a thermostat. The water level in the bath was maintained above the solution in the cell. The experiments were conducted at 273, 298, and 323 K, respectively.

In order to investigate the quasi-2-D zinc growth forms, we adopted the apparatus reported in Ref. 5. Two pieces of Perspex, 7.0 cm in diam, were secured by the anode zinc ring. A piece of cellulose filter paper was placed between two pieces of Perspex. The cathode was a Pt wire of 0.2 mm diam and electrolyte was $1 \text{ mol L}^{-1} \text{ Zn(Ac)}_2$. Under a constant potential of 2.0 V, the quasi-2-D zinc layers grown at 273 and 323 K were recorded by a video camera.

SEM samples of the zinc electrodeposited layer were prepared on carefully polished copper sheets 0.2 mm thick and of $1.5 \times 1.5 \text{ cm}$ area. In the solution of $0.1 \text{ mol L}^{-1} \text{ Zn(Ac)}_2$ with $0.5 \text{ mol L}^{-1} \text{ NaAc}$, the copper sheets were electroplated for 15 min with a constant current of 80 mA and agitation at 298 and 323 K, respectively, and the cell voltages were recorded simultaneously. The surface morphology of the deposited zinc film was observed by ISI-SX-40-type SEM.

All solutions were prepared from chemicals of analytical grade and triply distilled water, and deaerated by bubbling with N_2 for 10 min before use. A potentiostat (RDE4, Pine Instrument Co.) was used in all experiments.

Results and Discussion

Voltammetric experiments at different temperatures.—The CVs of a static mercury drop electrode in the solution of $0.1 \text{ mol L}^{-1} \text{ Zn(Ac)}_2$ with $0.5 \text{ mol L}^{-1} \text{ NaAc}$ at 273, 298, and 323 K are shown in Fig. 1, respectively. The potential was swept from -0.8 V going in the cathodic direction. The anodic part is ignored in this figure. The distinct feature of the CV curves in Fig. 1 is a single cathodic peak from -0.8 to -1.3 V . It indicates that the reduction of Zn^{2+} ions is a simple reaction at three temperatures and that the second electron reduction exhibits a very fast step. Under the condition of the half-infinite linear diffusion, the peak current i_p can be described by the following equation⁶⁻⁸

$$i_p = K_D c v^{1/2} \quad [1]$$

where c is the concentration of the active cation (mol cm^{-3}), v the scan rate (V s^{-1}), and K_D is a constant related to the properties of

^z E-mail: jxyu@whu.edu.cn

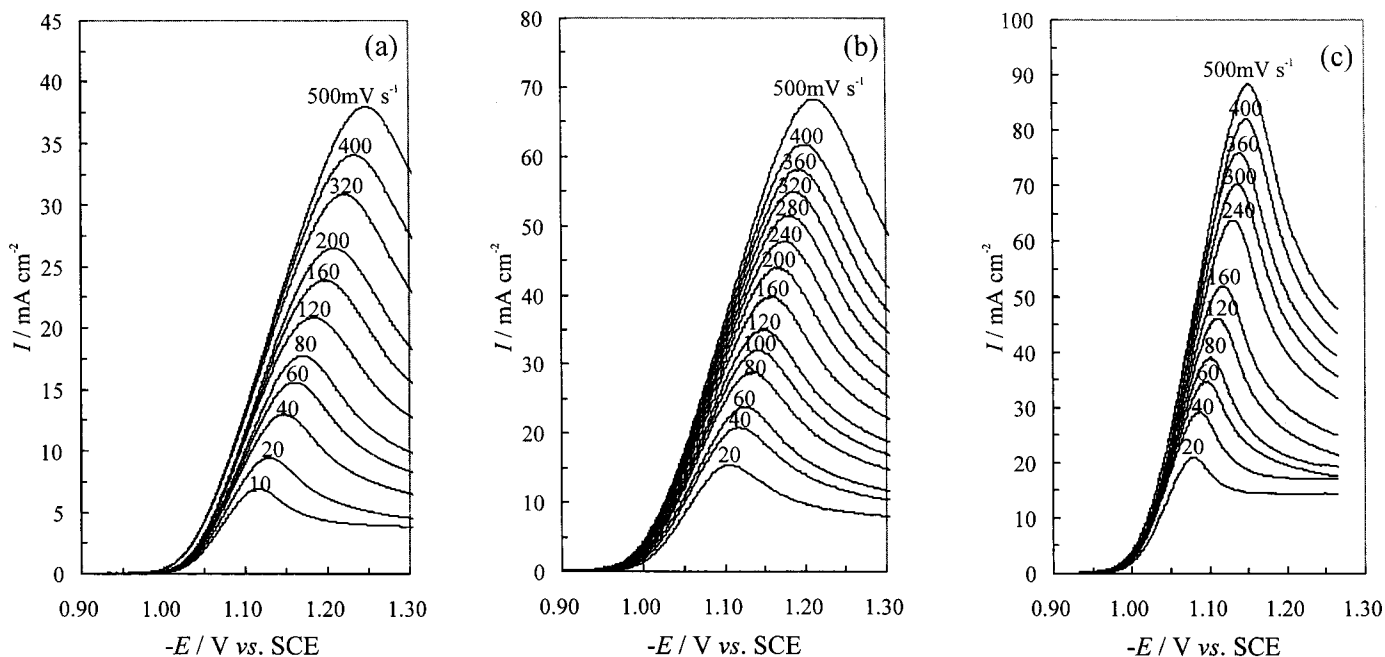


Figure 1. Cyclic voltammograms for Zn^{2+} ions on a static mercury drop electrode immersed in a solution of $0.1 \text{ mol L}^{-1} \text{ Zn}(\text{Ac})_2$ with $0.5 \text{ mol L}^{-1} \text{ NaAc}$ at different temperatures. The scan rates are labeled on each curve. (a) 273 K, (b) 298 K, and (c) 323 K.

the reaction system. For an irreversible reaction, K_D is equal to $2.99 \times 10^5 n(\alpha n_\alpha)^{1/2} AD^{1/2}$ and the relationship between i_p and the peak potential E_p is given by⁶

$$i_p = 0.227nFAck^0 \exp\left[-\left(\frac{\alpha n_\alpha F}{RT}\right)(E_p - E^0)\right] \quad [2]$$

where k is the conditional standard rate constant and E^0 is the equilibrium potential.

As shown in Fig. 2, the plot of i_p vs. $v^{1/2}$ is a straight line with a zero intercept on the current axis at each temperature. Moreover, an increase in temperature leads to a larger slope. This suggests that the Zn^{2+} reduction process is controlled by mass transfer. As depicted in Fig. 3, the plot of $\ln i_p$ vs. $E_{pc} - E_0$ is linear at each temperature and the intercept on the $\ln i_p$ axis increases with temperature. According to the slopes of these lines shown in Fig. 2 and 3, the values of D , α ,

and k at different temperatures were calculated, as listed in Table I. From this table, it can be seen that the values of D , α , and k increase with the temperature. The parameters obtained at 298 K are analogous to the values reported by other workers.⁹ Figure 4 shows the conditional standard rate constant as a function of temperature. These results reveal that an increase in temperature leads to a higher k and that the relation between $\log k$ and $1/T$ is linear. Based on the Arrhenius equation,^{10,11} the slope allows us to calculate the activation energy of the process using the following equation

$$\Delta H^\ddagger = 2.303R \frac{d \ln k}{d(1/T)} \quad [3]$$

where ΔH^\ddagger is the activation energy of the process. According to the

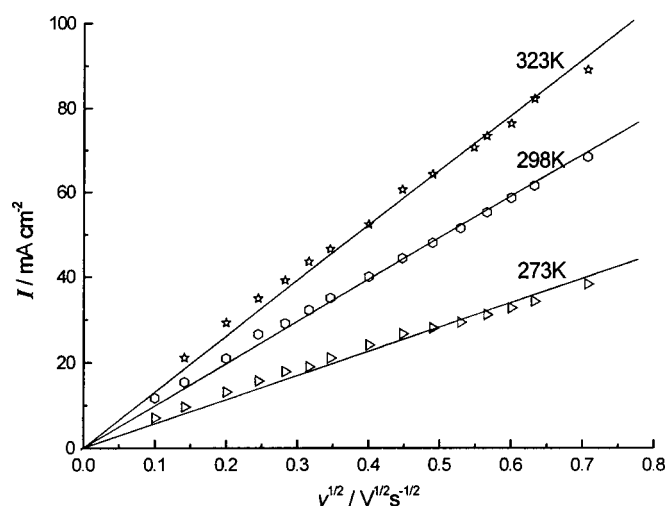


Figure 2. Plot of i_p vs. $v^{1/2}$ for the reduction of Zn^{2+} ions in a solution of $0.1 \text{ mol L}^{-1} \text{ Zn}(\text{Ac})_2$ with $0.5 \text{ mol L}^{-1} \text{ NaAc}$ at different temperatures.

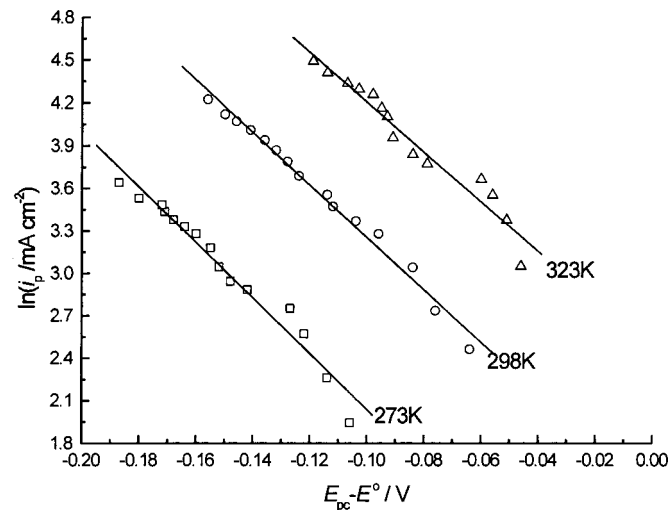


Figure 3. The plot of $\ln i_p$ vs. $E_{pc} - E_0$ for the reduction of Zn^{2+} ions at different temperatures.

Table I. The values of D , α , and k obtained at different temperatures.

| T (K) | D ($\text{cm}^2 \text{s}^{-1}$) | α | k (cm s^{-1}) |
|------------|--|----------|-------------------------------|
| 273 | 1.93×10^{-6} | 0.231 | 2.45×10^{-4} |
| 298 | 5.71×10^{-6} | 0.237 | 1.02×10^{-3} |
| 323 | 9.54×10^{-6} | 0.243 | 3.66×10^{-3} |

slope, we determine the activation energy of the $\text{Zn}^{2+} + 2\text{e}^- = \text{Zn}(\text{Hg})$ reaction to be $-39.662 \text{ kJ mol}^{-1}$, which is comparable to the value reported in Ref. 9-11.

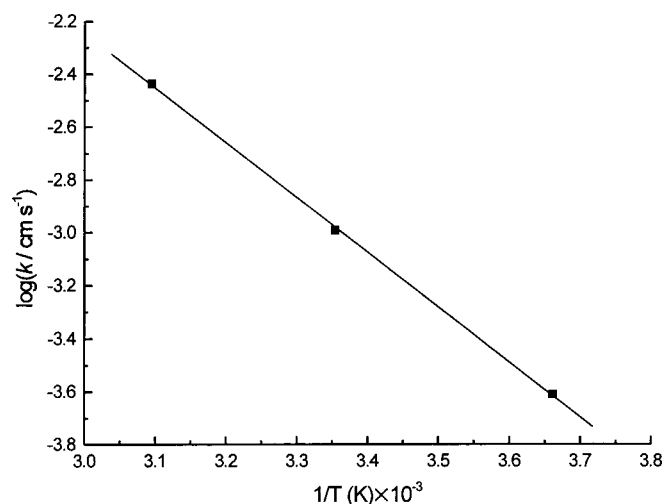
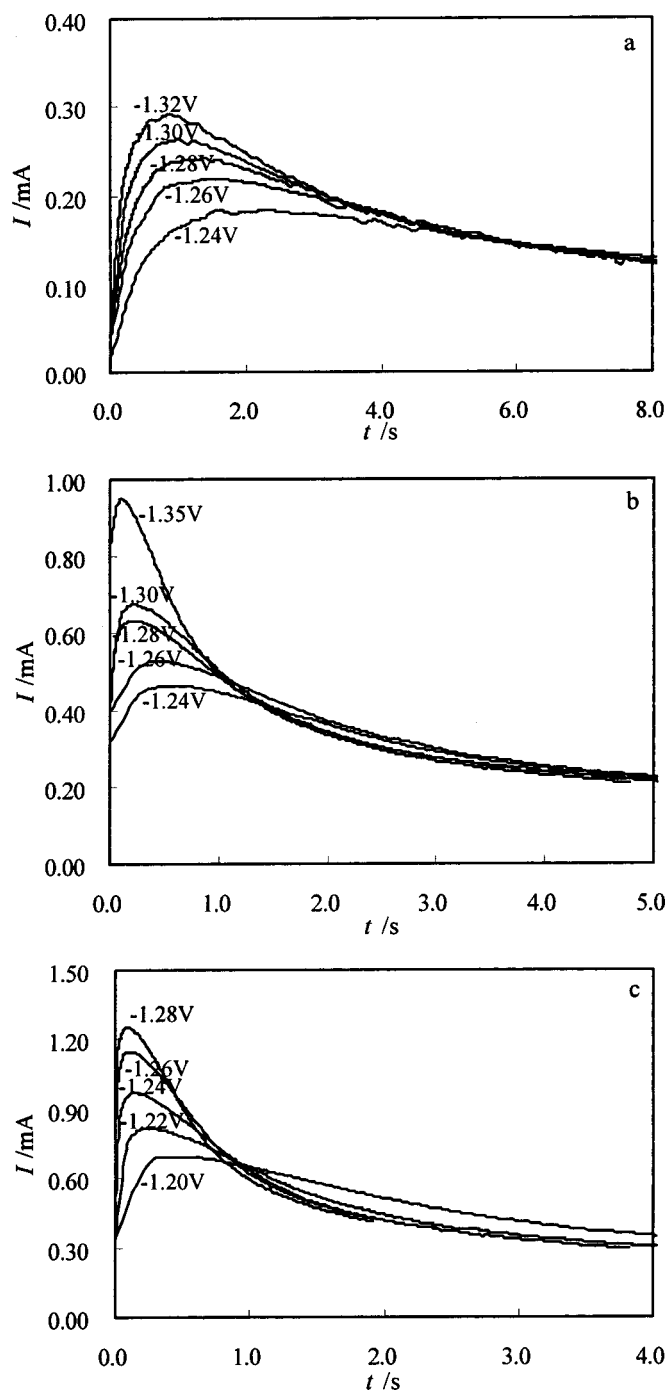
Chronoamperometric experiments at different temperatures.—Figure 5 shows three families of potentiostatic current/time transients for zinc electrodeposition onto GC electrode from a solution of $0.1 \text{ mol L}^{-1} \text{ Zn}(\text{Ac})_2$ with $0.5 \text{ mol L}^{-1} \text{ NaAc}$ at different temperatures. When a step potential E was employed, the current density first increased sharply to reach a maximum value I_m , at the time, t_m , and then gradually decayed with time as described by the Cottrell equation. At a constant temperature, the larger the amplitude of the potential step, the larger was I_m . For a given E , I_m grew with increasing temperature. In consideration of the overlapping of the diffusion fields of randomly growing nuclei, Scharifker and Mostany¹² deduced the following expression to describe the general potentiostatic current/time relations for nucleation and growth of an electrodeposit

$$I = \frac{zFD^{1/2}c}{\pi^{1/2}t^{1/2}} \left[1 - \exp\left(-N_0\pi kD\left\{t - \frac{[1 - \exp(-At)]}{A}\right\}\right) \right] \quad [4]$$

$$k \equiv (8\pi cM/\rho)^{1/2}$$

where z is the number of equivalents, D is the diffusion coefficient, c is the concentration of active cation, M is the atomic weight of the metal, ρ is the density of the deposit, N_0 is the nucleation density (cm^{-2}), and A is the nucleation rate constant ($\text{cm}^{-2} \text{s}^{-1}$).

In previous research, we have proposed a genetic algorithm to deal with the nucleation problem,¹⁵ where Eq. 4 can be regarded as the basic model structure, with A , N_0 , and D as estimated parameters. By using this algorithm to fit the whole current transient at different temperatures, we can optimize those parameters easily by choosing 500 data points as samples in the corresponding curves. Because it is a stochastic algorithm, 10 runs were conducted inde-

**Figure 4.** Relation between the conditional standard rate constant and the temperature.**Figure 5.** Potentiostatic current/time curves for zinc electrodeposition on a GC electrode from a solution of $0.1 \text{ mol L}^{-1} \text{ Zn}(\text{Ac})_2$ with $0.5 \text{ mol L}^{-1} \text{ NaAc}$ at three temperatures: (a) 273 K, (b) 298 K, and (c) 323 K. For each curve, the potential pulse starts from -1.0 V to the indicated potential.

pendently for each experimental current/time transient. We also calculate the square of the correlation coefficient r^2 to assess the fitting quality by the following formula

$$r^2 = 1 - \frac{\sum_{i=1}^m (I_i - \hat{I}_i)^2}{\sum_{i=1}^m (I_i - \bar{I})^2} \quad [5]$$

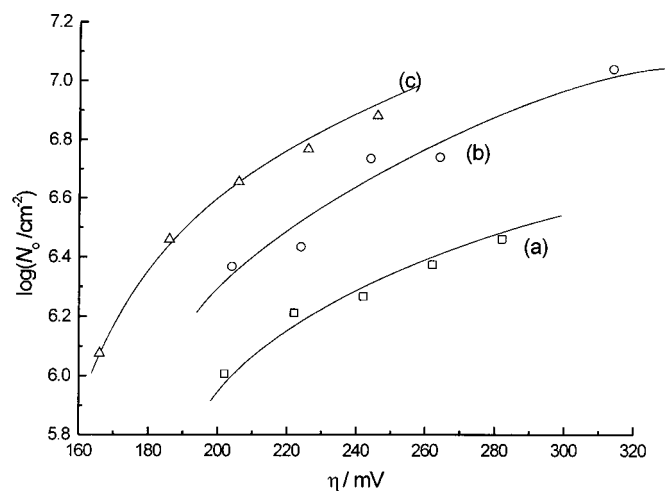
Table II. The values of D , A , N_0 , the fitting error, and the mean runtime at different temperatures.

| T (K) | E (V) | D ($\text{cm}^2 \text{s}^{-1}$) | N_0 (cm^{-2}) | A (s^{-1}) | Fitting error | r^2 |
|------------|------------|--|-------------------------------|----------------------------|-----------------------|-------|
| 273 | -1.24 | 1.185×10^{-6} | 1.02×10^6 | 1.41×10^9 | 8.9×10^{-6} | 0.99 |
| 273 | -1.26 | 1.123×10^{-6} | 1.63×10^6 | 1.41×10^9 | 1.05×10^{-5} | 0.99 |
| 273 | -1.28 | 1.161×10^{-6} | 1.85×10^6 | 1.41×10^9 | 1.05×10^{-5} | 0.99 |
| 273 | -1.30 | 1.121×10^{-6} | 2.37×10^6 | 1.41×10^9 | 1.18×10^{-5} | 0.99 |
| 273 | -1.32 | 1.124×10^{-6} | 2.89×10^6 | 1.41×10^9 | 9.65×10^{-6} | 0.99 |
| 298 | -1.24 | 2.109×10^{-6} | 2.33×10^6 | 1.41×10^9 | 1.42×10^{-4} | 0.97 |
| 298 | -1.26 | 2.230×10^{-6} | 2.72×10^6 | 1.41×10^9 | 3.10×10^{-4} | 0.95 |
| 298 | -1.28 | 1.924×10^{-6} | 5.44×10^6 | 1.41×10^9 | 5.48×10^{-4} | 0.95 |
| 298 | -1.30 | 2.010×10^{-6} | 5.50×10^6 | 1.41×10^9 | 3.59×10^{-4} | 0.95 |
| 298 | -1.35 | 2.040×10^{-6} | 1.09×10^7 | 1.41×10^9 | 9.82×10^{-4} | 0.94 |
| 323 | -1.20 | 4.328×10^{-6} | 1.19×10^6 | 1.41×10^9 | 1.45×10^{-4} | 0.97 |
| 323 | -1.22 | 3.326×10^{-6} | 2.88×10^6 | 1.41×10^9 | 2.27×10^{-4} | 0.96 |
| 323 | -1.24 | 3.224×10^{-6} | 4.51×10^6 | 1.41×10^9 | 8.78×10^{-4} | 0.94 |
| 323 | -1.26 | 3.394×10^{-6} | 5.84×10^6 | 1.41×10^9 | 2.87×10^{-4} | 0.95 |
| 323 | -1.28 | 3.234×10^{-6} | 7.60×10^6 | 1.41×10^9 | 2.11×10^{-4} | 0.96 |

where $\bar{I} = 1/m \sum_{i=1}^m I_i$. Table II lists the calculated values of D , A , r^2 , N_0 , and the fitting error for different step potentials.

As shown in Table II, the fitting errors for all of the experimental current/time transients are very small, and their r^2 values are all greater than 0.94. This indicates that the fitting curves coincide with the experimental current/time transients very well. Furthermore, the diffusion coefficients obtained for different step potentials are very consistent under the same temperature. The mean values of the diffusion coefficients at 273, 298, and 323 K are 1.14×10^{-6} , 2.10×10^{-6} , and $3.50 \times 10^{-6} \text{ cm}^2 \text{ s}^{-1}$, respectively. Obviously the diffusion coefficients increase slowly with an increase in temperature. It can also be seen that the D value obtained by chronoamperometry is lower than that obtained by the cyclic voltammetry at the same temperature. A similar phenomenon was observed by other researchers,¹⁴ but the reason for this result is not clear yet.

Using the values of N_0 listed in Table II, the dependence of $\log N_0$ vs. overpotential, η , is plotted in Fig. 6. From this figure, it is clear that N_0 has a strong dependence on η and T . That is, an increase in η or temperature leads to a higher value for N_0 . At a given η , N_0 at 298 K is two times larger than that at 273 K. This fact indicates that an increase in temperature facilitates the formation of new nuclei.

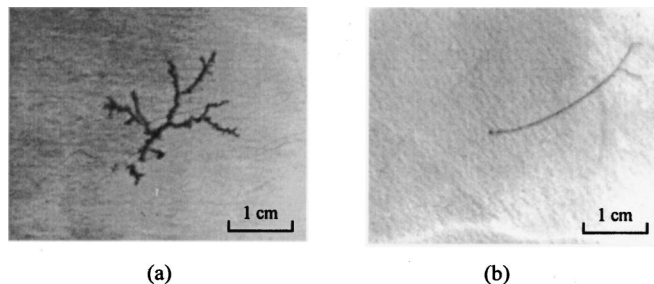
**Figure 6.** Plot of $\log N_0$ vs. η for zinc electrodeposition on a GC electrode at different temperatures: (a) 273 K, (b) 298 K, and (c) 323 K.

As shown in Table II, the nucleation rate constant, A , is very large at all three temperatures, about $1.41 \times 10^9 \text{ s}^{-1}$. According to the first order nucleation rate equation, the 3-D nucleation can be expressed as

$$N(t) = N_s [1 - \exp(-At)] \quad [6]$$

where N_s is the number of active sites on the substrate. This equation has two extreme cases. One case is $N(t) = N_s$ for a large A value which corresponds to instantaneous nucleation. The other is $N(t) = AN_s t$ for a small A value which corresponds to progressive nucleation. The large A value indicates that the mechanism of zinc electrocrystallization onto GC electrode at all three temperatures follows a 3-D instantaneous nucleation and growth model.

Fractal morphology of a quasi-2-D zinc deposit at different temperatures.—Under the constant cell potential of 2.0 V, the morphology of the quasi-2-D zinc deposition at 273 and 323 K were monitored, respectively, as shown in Fig. 7. From this figure, the random fractal morphology of zinc at 273 K exhibits isotropic growth with larger and thicker branches. In contrast, the fractal morphology of zinc at 323 K exhibits anisotropic growth with less and thinner branches. According to the diffusion-limited aggregation (DLA) model, in an electric field, the Zn^{2+} ions in the solution diffuse and discharge randomly once they encounter the growing cluster. They first form adatoms by obtaining electrons and then are trapped immediately with no further diffusion. This model can account for the ramified structure of zinc growth, but cannot explain the variation of branch width. In fact, the 2-D zinc growth in a practical solution is much more complicated. Röder¹⁵ demonstrated that the adatoms attached to the growing cluster can continue to

**Figure 7.** The fractal morphology of quasi-2-D zinc deposition at different temperatures at a constant potential of 2.0 V. (a) 273 K, (b) 323 K.

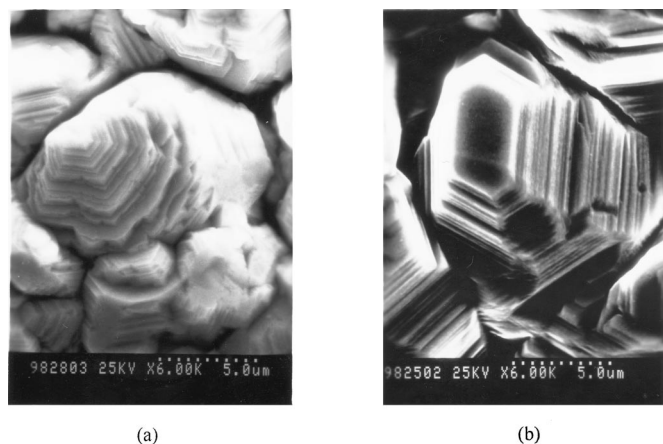


Figure 8. Scanning electron micrographs for zinc films deposited from a solution of $0.1 \text{ mol L}^{-1} \text{ Zn}(\text{Ac})_2$ with $0.5 \text{ mol L}^{-1} \text{ NaAc}$ onto $1.5 \times 1.5 \text{ cm}$ copper sheets. (a) 273 K, (b) 323 K.

migrate and reach the stable sites with more coordination points. According to the previous chronoamperometric experiments, the diffusion coefficient of Zn^{2+} ions and the nucleation density increase with the increasing of temperature. It means that Zn^{2+} ions obtain electrons and form adatoms more quickly at a higher temperature. On the other hand, the edge diffusion rate of adatoms grows exponentially when the temperature increases. At 273 K, because the edge diffusion rate is low, a large amount of adatoms are produced before the earlier adatoms migrate and reach the stable sites. This makes the mobile adatoms attach mutually and form plenty of new kinks. Thus, the fractal morphology of a zinc deposit exhibits isotropic growth with more and thicker branches. In contrast, at 323 K, because the edge diffusion of adatoms accelerates exponentially, the production rate of adatoms is relatively slow. This makes the adatoms more likely to diffuse and reach the stable sites. Thus, the fractal morphology of these zinc deposits exhibits anisotropic growth with fewer and thinner branches.

Microstructure of the deposited zinc film.—Under a constant current of 80 mA and with agitation, zinc films were deposited on copper sheets at 273 and 323 K. A significant difference in the bath potential at 273 and 323 K can be observed, with 3.50 and 1.20 V, respectively. This indicates that the increase of temperature helps to reduce the polarization of Zn^{2+} ions reduction. Figure 8 shows the SEM micrographs for deposited zinc films at 273 and 323 K, respectively. From these two micrographs, the growth direction of grains is parallel to the substrate, and grains are regular and symmetrical with a series of plate-like crystals stacked up mutually like a pagoda. Similar results were obtained by Zhou⁴ and Yan¹⁶ when they investigated the electrodeposition of zinc in sulfate solutions. Nevertheless, the difference between these two micrographs is obvious. In Fig. 8a, plate-like crystals develop unintegrally like irregular hexagonal crystallites. But this type of defect cannot be observed in Fig. 8b. According to Kossel's theory and the previous results in this

paper, and because the diffusion rate of surface adatoms is slow at 273 K, a part of the adatoms cannot diffuse and reach the stable sites simultaneously. This causes the earlier adatoms to be encased by new adatoms and to form new kinks. Thus, plate-like crystals grow unintegrally. On the contrary, because the diffusion rate of surface adatoms accelerates exponentially at 323 K, the production rate of adatoms is relatively slow. Thus, the grains develop integrally and adequately.

Conclusion

From the results of cyclic voltammetry experiments at different temperatures, we calculated the kinetic parameters D , α , and k for the $\text{Zn}^{2+} + 2e^- = \text{Zn}(\text{Hg})$ reaction. Based on the slope of $d \ln k/d(1/T)$, we determined the activation energy of this reaction to be $-39.662 \text{ kJ mol}^{-1}$.

Chronoamperometric experiments showed that the nucleation density increases when the temperature increases. Moreover, the nucleation rate constant is always very large at all temperatures, about $1.41 \times 10^9 \text{ s}^{-1}$.

The fractal morphology of zinc exhibits isotropic growth with more and thicker branches at 273 K. In contrast, the fractal morphology of zinc exhibits anisotropic growth with fewer and thinner branches at 323 K. Similarly, the microstructure of zinc deposits shows that plate-like crystals grow unintegrally like irregular hexagonal crystallites at 273 K, but the grains develop integrally and adequately at 323 K.

Acknowledgments

This work was partially supported by the Chinese National Natural Science Foundation (no. 29833090). The authors would like to thank Professor Charles L. Hussey for his helpful comments and efforts in improving the English and style of this paper.

References

1. J. X. Yu, Y. Y. Chen, and Q. A. Huang, *Wuhan Daxue Xuebao, Ziran Kexuebao*, **42**, 686 (1996).
2. J. X. Yu, Y. Y. Chen, Q. A. Huang, and H. X. Yang, *Gaodeng Xuexiao Huaxue Xuebao*, **20**, 107 (1999).
3. J. X. Yu, Y. Y. Chen, H. X. Yang, and Q. A. Huang, *J. Electrochem. Soc.*, **146**, 1789 (1999).
4. F. Y. Ge, Y. Z. Zhang, S. B. Yao, S. K. Xu, and S. M. Zhou, *Gaodeng Xuexiao Huaxue Xuebao*, **16**, 87 (1995).
5. S. N. Atchison, R. P. Burford, and D. B. Hibbert, *J. Electroanal. Chem.*, **371**, 137 (1994).
6. A. J. Bard and L. R. Faulkner, *Electrochemical Methods: Fundamentals and Applications*, John Wiley & Sons, Inc., New York (1980).
7. R. S. Nicholson and I. Shain, *Anal. Chem.*, **36**, 706 (1964).
8. C. S. Cha, *Introduction to Kinetics of Electrode Processes*, China Academic Press, Beijing (1987).
9. R. J. Brodd and V. E. Leger, in *Encyclopedia of Electrochemistry of the Elements*, A. J. Bard, Editor, Vol. V, Marcel Dekker, Inc., New York (1976).
10. N. S. Hush and J. Blackledge, *J. Electroanal. Chem.*, **5**, 420 (1963).
11. J. Blackledge and N. S. Hush, *J. Electroanal. Chem.*, **5**, 435 (1963).
12. B. R. Scharifker and J. Mostany, *J. Electroanal. Chem. Interfacial Electrochem.*, **177**, 13 (1984).
13. J. X. Yu, H. Q. Cao, Y. Y. Chen, L. S. Kang, and H. X. Yang, *J. Electroanal. Chem.*, **474**, 69 (1999).
14. M. Palomar-Pardave, M. T. Ramirez, I. Gonzalez, A. Serruya, and B. R. Scharifker, *J. Electrochem. Soc.*, **143**, 1551 (1996).
15. H. Röder, K. Bromann, and H. Brune, *Phys. Rev. Lett.*, **74**, 3217 (1995).
16. H. Yan, J. Downes, P. J. Boden, and S. J. Harris, *J. Electrochem. Soc.*, **143**, 1577 (1996).